AGU ADVANCING EARTH AND SPACE SCIENCE

Geophysical Research Letters®

RESEARCH LETTER
10.1029/2022GL101480

# Fast and Slow Subpolar Ocean Responses to the North Atlantic Oscillation: Thermal and Dynamical Changes

**Hemant Khatri[1], Richard G. Williams[1], Tim Woollings[2], and Doug M. Smith[3]**

[1]Department of Earth, Ocean and Ecological Sciences, School of Environmental Sciences, University of Liverpool, Liverpool, UK, [2]Department of Physics, University of Oxford, Oxford, UK, [3]Met Office, Hadley Centre, Exeter, UK

**Key Points:**

- Subpolar ocean changes due to the North Atlantic Oscillation (NAO) are separated into competing fast, seasonal and slow, inter-annual responses
- Fast response is related to the anomalous Ekman transport and air-sea heat exchange associated with the NAO
- Slow response is due to the redistribution of subtropical temperature anomalies via overturning and gyre circulations

**Supporting Information:**

Supporting Information may be found in the online version of this article.

**Correspondence to:**

H. Khatri,
hkhatri@liverpool.ac.uk

**Citation:**

Khatri, H., Williams, R. G., Woollings, T., & Smith, D. M. (2022). Fast and slow subpolar ocean responses to the North Atlantic Oscillation: Thermal and dynamical changes. *Geophysical Research Letters*, *49*, e2022GL101480. https://doi.org/10.1029/2022GL101480

Received 27 SEP 2022
Accepted 7 DEC 2022

**Author Contributions:**

**Conceptualization:** Richard G. Williams, Tim Woollings
**Data curation:** Hemant Khatri, Doug M. Smith
**Formal analysis:** Hemant Khatri
**Funding acquisition:** Richard G. Williams
**Methodology:** Hemant Khatri, Richard G. Williams, Tim Woollings, Doug M. Smith
**Software:** Hemant Khatri
**Supervision:** Richard G. Williams
**Writing – original draft:** Hemant Khatri



**Abstract** Climate model hindcasts are analyzed to reveal the impacts of the North Atlantic Oscillation (NAO) on the North Atlantic subpolar ocean, which exhibits variability on seasonal to decadal timescales. The ocean response to a single winter NAO event is separated into fast and slow responses. The fast response persists over winter–spring seasons, during which wind stress and heat flux anomalies associated with the NAO rapidly modify ocean temperatures via changes in Ekman transport and ocean-atmosphere heat exchanges. The slow response persists for 3–4 years, during which overturning and gyre circulations redistribute opposing-signed surface temperature anomalies created by the NAO. This redistribution modifies east-west temperature contrasts altering the meridional heat transport associated with gyres and changing the strength of the overturning circulation. Hence, the fast and slow responses lead to opposing-signed subpolar temperature anomalies in time from the competing effects of local forcing and horizontal heat convergence.

**Plain Language Summary** The North Atlantic Oscillation (NAO) index is one of the most common metrics to characterize atmospheric regimes in the northern hemisphere, revealing how different patterns of atmospheric winds and air-sea fluxes over Europe and North America affect the ocean state. In the present research, coupled climate model simulations are utilized to study the impacts of particular atmospheric events on the subpolar North Atlantic Ocean. Using NAO indices during the winter season, sets of multiple simulations having similar types of atmospheric events are created to carry out a composite analysis. The analyses reveal that the impact of atmospheric events on the oceans can last up to 4–5 years (or even longer in some cases). The fast response is controlled by the effect of the local winds and air-sea heat fluxes, while the slow response is related to the role of the meridional overturning circulation and ocean gyres in transporting heat anomalies from the subtropics to the subpolar ocean. The combination of these fast and slow responses leads to the sign reversal of the subpolar surface temperature anomalies in time.

## 1. Introduction

Ocean observations and historical reconstructions of the ocean state reveal significant inter-annual and decadal variability in the overturning circulation and ocean heat content for the North Atlantic (Fraser & Cunningham, 2021; Jackson et al., 2022; Lozier et al., 2008; Roussenov et al., 2022; Williams et al., 2014). These variations are primarily driven by variability in the atmospheric forcing through exchanges of momentum and buoyancy (Eden & Jung, 2001; Josey & Sinha, 2022) with different imprints for a range of atmospheric regimes (Barrier et al., 2014). Unlike in the atmosphere, ocean memory can last for a few years (Hansen & Bezdek, 1996), potentially giving a long-term effect on the climate state.

This study investigates the impacts of atmospheric variability on the ocean state in the subpolar North Atlantic associated with the North Atlantic Oscillation (NAO) (Hurrell, 1995; Hurrell & Deser, 2010), which is the dominant mode of atmospheric variability in the Atlantic sector. NAO events significantly affect the magnitudes and spatial patterns of surface winds and air-sea fluxes (Marshall, Kushnir, et al., 2001; Visbeck et al., 1998). For example, in the positive phase of the NAO, the atmospheric jet strengthens and shifts poleward (Woollings et al., 2010) resulting in anomalously strong surface winds and more heat loss from the subpolar ocean to the atmosphere. These anomalous wind and buoyancy forcings then affect the ocean heat content and meridional overturning circulation (Lozier et al., 2008, 2010; Marshall, Johnson, & Goodman, 2001; Williams et al., 2014).

The oceans respond to NAO forcing on seasonal to decadal timescales (Eden & Willebrand, 2001; Lohmann et al., 2009b). The immediate ocean response to an NAO event involves changes in surface temperatures from air-sea heat flux anomalies and wind-induced changes in Ekman transport (Barrier et al., 2014; Eden

**Writing – review & editing:** Hemant Khatri, Richard G. Williams, Tim Woollings, Doug M. Smith

& Willebrand, 2001; Marshall, Johnson, & Goodman, 2001). There is also a delayed ocean response involving changes in the meridional overturning circulation and heat transport on inter-annual to decadal timescales (Robson et al., 2012; Williams et al., 2015). However, there are uncertainties about the controlling mechanisms and the timing of the delayed ocean response.

The delayed ocean response to NAO forcing may be related to the strength of the gyre and overturning circulations, and the resulting heat convergence, in the subpolar region (Lozier et al., 2010; Williams et al., 2015; Yang et al., 2016). Surface wind anomalies due to NAO forcing alter the gyre strength, which then modifies east-west pressure gradients resulting in changes in the meridional overturning and associated heat transport (Eden & Willebrand, 2001; Zhao, 2017). Alternatively, variability in the deep water formation rates in Irminger and Labrador seas also impacts the overturning strength on inter-annual timescales (Desbruyères et al., 2019; Menary et al., 2020; Robson et al., 2016; Yeager et al., 2021). The temporal variability in the overturning circulation may be a delayed response to NAO forcing, as suggested for sea surface temperatures (SSTs) and overturning in the North Atlantic with time lags in the range of 2–20 years (Fraser & Cunningham, 2021; Kloewer et al., 2014; O'Reilly et al., 2019; Robson et al., 2016; Yeager et al., 2021; Zou et al., 2020).

In the present work, the impacts of winter NAO forcing on the subpolar North Atlantic Ocean are examined on seasonal to inter-annual timescales using climate model ensemble prediction experiments. The novel aspect is that composites of selected ensemble simulations are employed to study the immediate and delayed ocean responses to a single NAO event, rather than a persistent change in NAO forcing. This multi-ensemble approach is effective in studying the coupled atmosphere-ocean variability without running NAO-perturbation experiments and interfering with model physics. To understand the controlling mechanisms, variations in the upper ocean heat content, overturning circulation, and heat transport are analyzed in both depth and density coordinates.

## 2. Model Description and Methodology

The analysis uses Met Office Decadal Climate Prediction System version 4 (DepreSys4) hindcasts, which are initialized using realistic atmospheric and oceanic states created from global ocean covariance analyses (Smith & Murphy, 2007) and ERA-interim reanalysis output (Dee et al., 2011). In each initialization, an ensemble of 10 members is created using the Met Office statistical ocean reanalysis (Smith et al., 2015) with covariance uncertainties sampled using different perturbed physics and forced ocean versions of the model. These ensemble members are initialized on 1st November every year (1960–2016) and are run for 125 months. DePreSys4 output has a resolution of 0.83° × 0.55° with 85 pressure levels in the atmosphere and 0.25° with 75 quasi-horizontal levels in the oceans. Anomalies in the available monthly diagnostics and offline-calculated diagnostics, for example, meridional overturning, northward heat transport, are computed by subtracting the model time-mean computed over 1979–2016 while keeping the lead time information of 125 months (Appendix E in Boer et al., 2016). In this approach, the model mean is a function of lead time, and the model drift contribution is appropriately removed in anomaly calculations.

The present study focuses on the subpolar North Atlantic Ocean variability associated with a single NAO event. All hindcasts are treated to be the same irrespective of the start date and there are 57 × 10 (number of years × ensemble) members in total. A subset of members is isolated based on seasonal mean NAO indices computed by taking the difference between the mean sea level pressure anomalies between Azores (36°N–40°N, 28°W–20°W) and Iceland (63°N–70°N, 25°W–16°W) regions. The NAO+ or NAO− subset comprises members that have a DJF seasonal-mean NAO index greater than 13 hPa or less than −13 hPa. The members are selected based on NAO indices in the second, third or fourth winter, and these members are further aligned along the time axis such that each of the selected members experiences the onset of an NAO event at the same time. The cut-off value of 13 hPa is twice the standard deviation of seasonal NAO indices in DePreSys4. There are 114 members for the NAO+ case and 133 members for the NAO− case. Apart from the timing of the NAO onset imposed in the selection process, the selected ensemble members are very different from each other in terms of the initial conditions of the atmospheric and ocean states, for example, pressure, velocity, and temperature fields, so that there is no bias in the ensemble selection.

Based on our criteria, all selected members are in a positive or negative NAO phase at year = 0 (Figures 1a–1b). These members are randomly distributed in terms of their NAO phases at all other times, which indicates that the atmospheric memory does not last longer than a few weeks. In a NAO+ phase, there are positive anomalies in

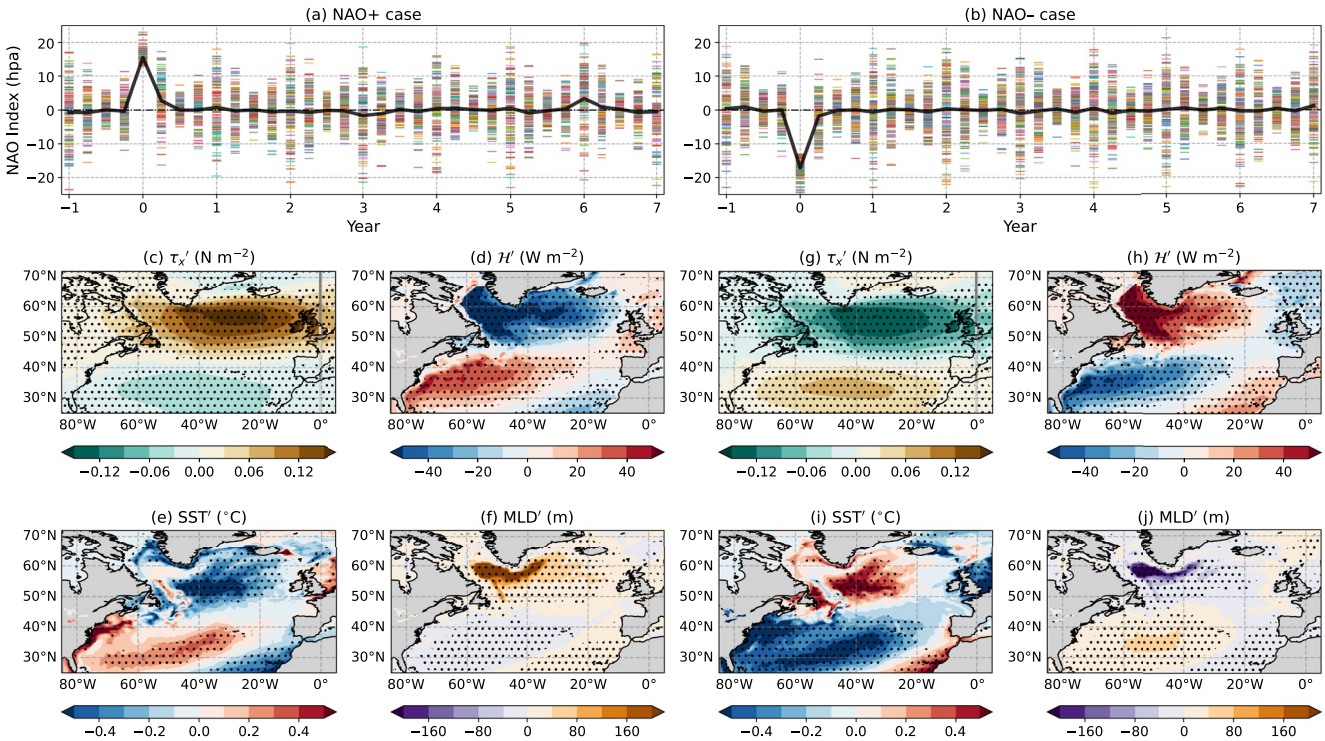


**Figure 1.** Composites of NAO+ and NAO− ensembles (a, b) Time-series of seasonal-mean North Atlantic Oscillation (NAO) indices for the selected members (year = 0 corresponds to DJF season and black curves represent the ensemble-mean NAO indices); (c–j) Mean surface ocean properties (DJFM season) in the NAO+ phase (left two columns) and in the NAO− phase (right two columns); (c, g) Zonal surface wind stress anomaly, $\tau_x'$; (d, h) Surface heat flux anomaly, $\mathcal{H}'$ (positive values indicate heat transfer from the atmosphere to the oceans); (e, i) Sea surface temperature anomaly, SST′; and (f, j) Mixed-layer depth anomaly, MLD′. Stippling denotes that anomalies are significant at 95% confidence level (computed using the bootstrapping method, Thomson & Emery, 2014). Anomalies are with respect to the mean over 1979–2016 (see Section 2).

the eastward wind stress northward of 45°N and negative anomalies southward of 45°N (Figure 1c). There is an associated negative-positive anomaly pattern in the air-sea heat flux (Figure 1d) with the oceans losing more heat to the atmosphere in the subpolar region and gaining more heat in the subtropics (Marshall, Kushnir, et al., 2001). As a result, negative SST anomalies and positive anomalies in mixed-layer depth initially occur in the subpolar ocean (Figures 1c–1d). In a NAO− phase, there is an opposing-signed response (Figures 1g–1j).

## 3. Composite Analysis of the Ensemble Subsets

The ocean response to anomalous wind stress and heat flux forcing due to winter NAO events (referred to henceforth as "NAO forcing") is analyzed in terms of an ocean heat budget interpreted in terms of the meridional overturning circulation and heat transport.

### 3.1. Heat Budget Analysis

The temporal evolution of SST anomalies is first analyzed in the NAO+ case (Figure 2a). For a NAO+ event in January to February of lag year = 0, there is a characteristic cooling northwards of 45°N and warming southwards of 45°N (Marshall, Kushnir, et al., 2001). However, the resulting negative SST anomalies in the subpolar ocean only persist for a year, and instead, positive SST anomalies develop at a lag of 2–4 years over most of the subpolar ocean.

A heat budget analysis is carried out to reveal the mechanisms that cause the changes in the upper ocean heat content. Ocean heat content anomaly (integrated between the surface and depth $z_o$) and an approximate upper ocean heat budget balance are given as

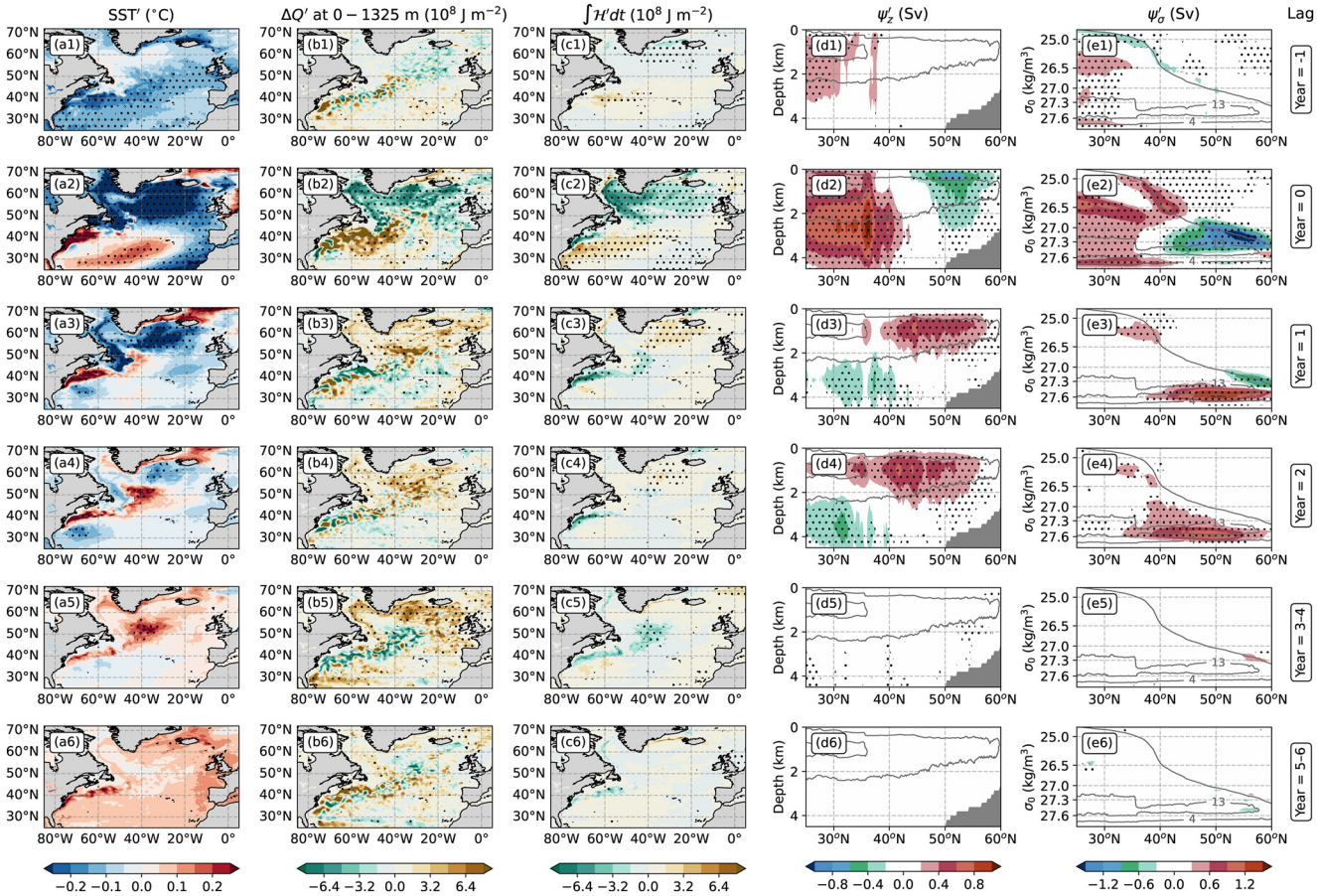


**Figure 2.** Temporal evolution of the ocean state in the NAO+ case (Composites of annual or bi-annual means from January to December are shown) (a1–a6) Sea surface temperature anomaly; (b1–b6) Heat content change in the upper 1,325 m (between January and December, i.e., $\Delta Q' = Q'_{Dec} - Q'_{Jan}$) in individual lag year periods; (c1–c6) Contribution from surface heat flux to the heat content change in individual lag year periods; (d1–d6) Anomaly in the overturning circulation in $z-$space; and (e1–e6) Anomaly in the overturning circulation in $\sigma-$space. Gray contours (are at 4 Sv and 13 Sv) in (d, e) represent the mean overturning circulation over 1979–2016 and all lead times. Lag represents the year from the onset of the NAO+ event, which occurs in January to February of lag year = 0. Stippling denotes that the change is significant at 80% confidence level. Anomalies are with respect to the mean over 1979–2016 (see Section 2).

$$Q'(x,y,t) = \rho_o C_p \int_{-z_o}^{0} \theta'(x,y,z,t)\mathrm{d}z, \tag{1}$$

$$\frac{\partial Q'}{\partial t} \approx \mathcal{H}' - \rho_o C_p \int_{-z_o}^{0} \nabla \cdot (\theta \mathbf{u})' \mathrm{d}z, \tag{2}$$

where $\theta$ is the potential temperature, prime represents the anomaly in a diagnostic field, $\mathbf{u} = (u, v, w)$ is the velocity field and $\nabla = (\partial_x, \partial_y, \partial_z)$ is the gradient operator, $\rho_o C_p$ and $z_o$ are set to $4.09 \times 10^6$ J K$^{-1}$m$^{-3}$ and 1,325 m as a rough measure of the thermocline depth, respectively. The upper ocean heat content change in Equation 2 is driven by two processes—surface forcing via the air-sea heat flux, $\mathcal{H}'$, and heat convergence (second term on the right). Additional heat diffusion and advective parameterization terms are needed to close the heat budget equation (Hieronymus & Nycander, 2013), and their contributions, which are diagnosed as a residual in Equation 2, only reach 10% in our analysis.

Consistent with the evolution of SST anomalies in the subpolar region, the upper ocean heat content declines in year 0 due to intense surface cooling, but gradually increases in years 1–4 after the onset of a NAO+ event (Figures 2b and 2c), the figure for the NAO− case is in Supporting Information S1. The two opposing-signed responses in the subpolar ocean are more clearly seen in the time-series of anomalies in SST and heat budget terms (Figures 3a, 3b, 3g, and 3h, gray shading indicates the periods of the initial and delayed responses). For

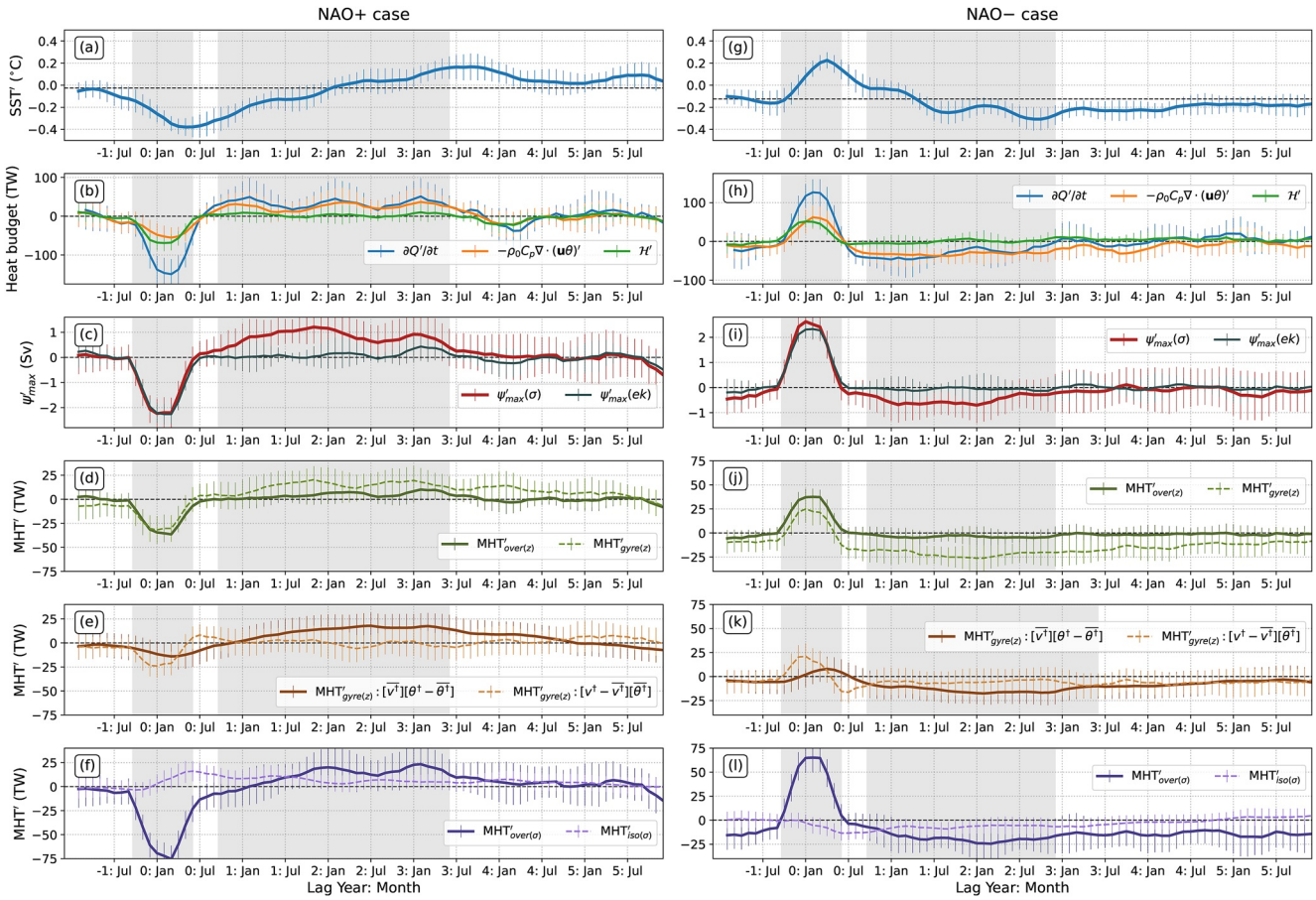


**Figure 3.** Composite-mean time-series (6-month running window is applied) for NAO+ and NAO− ensembles (a, g) Domain-mean sea surface temperature anomaly; (b, h) Anomalies in heat budget (integrated in the upper 1,325 m and over the selected domain); (c, i) Anomalies in the overturning maximum, $[\max(\psi(\sigma))]'$, and Ekman transport at 50°N; and (d–f, j–l) Anomalies in full-depth-integrated meridional heat transport at 50°N. Time-series plots in (a, b, g, h) are for the region bounded between 45°N–60°N and 50°W–20°W. Errorbars indicate the 95% confidence intervals.

example, in the NAO+ case, the initial reduction in SST happens within a period of a few months, whereas the subsequent increase in SST occurs over 2–3 years. Similarly, the initial rapid increase and subsequent slow decrease in SST are evident in the NAO− case.

During the fast-response period, both surface heat flux and heat convergence contribute about equally to the heat content change (Figures 3b and 3h). The zonal wind stress anomalies associated with NAO events result in anomalous heat convergence. For example, in the NAO+ case, positive zonal wind stress anomalies drive more southward Ekman transport in the subpolar region, which leads to anomalous cooling in the ocean surface layer (see Eden & Willebrand, 2001). Thus, on seasonal timescales, anomalies in both surface wind and buoyancy forcing are important in determining the variations in the upper ocean heat content in the subpolar North Atlantic. During the slow-response period, however, heat convergence provides the primary control of upper ocean heat content anomalies, and the change in the sign of subpolar SST anomalies with time is due to the transport of opposing-signed SST anomalies from the subtropical ocean into the subpolar ocean (Figures 3a, 3b, 3g, and 3h). A NAO+ event results in delayed warming and a NAO− event results in delayed cooling in the subpolar North Atlantic ocean. These fast and slow ocean responses to NAO forcing are broadly in accord with results from idealized modeling experiments (Eden & Willebrand, 2001; Lohmann et al., 2009b), as well as analyses from realistic climate model simulations and ocean reanalysis products (Robson et al., 2012). However, the timescale associated with the slow ocean response in our analysis differs from the timescale observed in idealized experiments (see Section 3.3).

There are notable spatial differences in the delayed ocean response between the NAO+ and NAO− cases. First, the delayed warming in the upper subpolar ocean due to NAO+ forcing is located around 40°W−30°W, whereas

the delayed cooling due to NAO− forcing appears to be further east at 30°W–20°W. In addition, during the slow-response period, persistent negative heat content anomalies occur at depths below 1,325 m in the NAO+ case, whereas there are no significant thermal signals at such depths in the NAO− case (see Supporting Information S1).

### 3.2. Meridional Overturning and Northward Heat Transport

The impacts of winter NAO forcing on meridional overturning circulation and heat transport are now assessed in depth ($z-$space) and density ($\sigma-$space) coordinates. The meridional overturning, $\psi$, is evaluated as,

$$\psi(y,s,t) = \int_{s_{\min}}^{s}\int_{x_w}^{x_e} \left(v(x,y,s,t) - \langle \underline{v} \rangle (y,t)\right) \mathrm{d}x\mathrm{d}s, \tag{3}$$

where $s$ represents the vertical coordinate ($z$ or $\sigma$ here), $\sigma$ is the potential density (referenced to 0 dbar pressure), $x_w$ and $x_e$ are the western and eastern boundaries of the ocean domain. $\langle \underline{v} \rangle$ is the zonal and depth average of the meridional velocity. Here, $v - \langle \underline{v} \rangle$ is used in the overturning calculation to ensure that overturning vanishes at vertical boundaries and there is net zero meridional volume transport. As expected, the meridional overturning circulation is stronger in $\sigma-$space than in $z-$space in the subpolar region (Figures 4a and 4g), also see Johnson et al. (2019), Lozier et al. (2019).

In the NAO+ case, there is a weakening in the overturning circulation in year 0 in the subpolar region, whereas the overturning circulation in the subtropics strengthens (Figures 2d–2e). The magnitude of the overturning circulation increases in the subsequent years at latitudes north of 40°N, which is close to the boundary between the subpolar and subtropical gyres. The initial weakening in subpolar overturning is due to anomalous Ekman transport and only lasts for a year, but the delayed strengthening lasts for 2–3 years. This persistent stronger overturning is the reason for more heat convergence and upper ocean warming in the subpolar region (Figures 3a and 3b). Hence, these two contrasting responses in the overturning are consistent with the fast and slow responses revealed in SST anomalies and the heat budget analysis.

Further, anomalies in Ekman volume transport, $\psi'(ek)$, due to zonal wind stress anomalies are computed,

$$\psi'(ek) = -\frac{1}{f\,\rho_o}\int_{x_w}^{x_e} \tau_x' \mathrm{d}x, \tag{4}$$

where $\rho_o = 1{,}035$ kg m$^{-3}$ is the reference density and $f$ is the Coriolis parameter. From the time-series of anomalies in the maximum overturning and Ekman transport at 50°N (Figures 3c and 3i), the rapid change in the overturning strength is associated with Ekman transport anomalies (also see Eden & Willebrand, 2001). In the slow-response period, the Ekman transport contribution is negligible, so the overturning anomalies correspond to the geostrophic flow component. In the NAO+ case, the initial weakening in the overturning is primarily surface intensified, whereas the delayed strengthening in the overturning occurs at depths of 1–2 km (Figure 2d). The initial weakening and subsequent strengthening in the overturning occur in different density layers (Figure 2e), consistent with the overturning anomalies in the slow-response period being associated with the geostrophic flow component. Essentially, ocean currents redistribute the surface buoyancy anomalies created by the NAO forcing leading to changes in east-west density contrasts and the associated geostrophic meridional overturning (Roussenov et al., 2022).

The ocean response is further analyzed in terms of meridional heat transport (MHT) in both depth and density coordinates. In $z-$space, the heat transport is decomposed into meridional overturning and horizontal gyre components. In $\sigma-$space, the heat transport is decomposed into meridional overturning and isopycnal components. The overturning heat transport is due to northward-moving warm waters in the upper limb and southward-moving cold waters in the lower limb. In contrast, gyre and isopycnal heat transports are due to northward and southward flows of different temperatures on the same depth and isopycnal levels, respectively. To perform this decomposition, the meridional velocity and potential temperature are separated into zonal-mean barotropic ($\langle \underline{v} \rangle$, $\langle \underline{\theta} \rangle$), zonal-mean baroclinic ($\langle v \rangle^{|}$, $\langle \theta \rangle^{|}$), and zonal anomaly ($v^{\dagger}$, $\theta^{\dagger}$) components in $z-$space, as well as in $\sigma-$space (Hall & Bryden, 1982; Siedler et al., 2001),

$$v(s,x,y,t) = \langle \underline{v} \rangle (y,t) + \langle v \rangle^{|}(s,y,t) + v^{\dagger}(s,x,y,t), \tag{5}$$

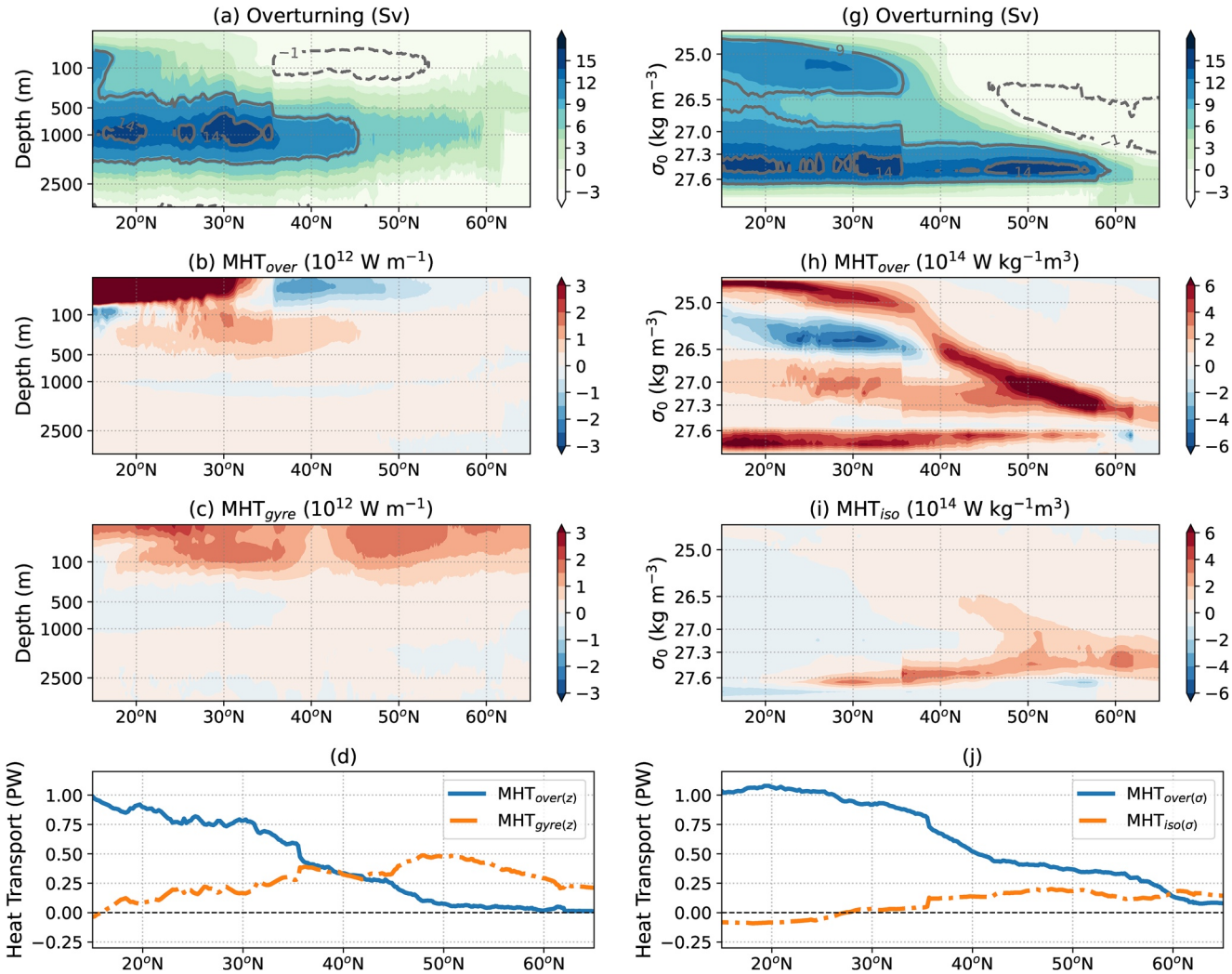


**Figure 4.** Depth and density-based views of the meridional overturning and northward heat transport from DePreSys4 data: Climatology (mean over 1979–2016 and all lead times) of (a, g) Overturning circulation; (b, c) Heat transport (per unit depth) due to overturning and gyre circulations in $z-$space; (h, i) Heat transport (per unit density) due to overturning and isopycnal circulations in $\sigma-$space; and (d, j) Vertically integrated heat transport in $z-$space and $\sigma-$space.

$$\theta(s,x,y,t) = \langle \underline{\theta} \rangle (y,t) + \langle \theta \rangle^{|}(s,y,t) + \theta^{\dagger}(s,x,y,t), \tag{6}$$

where $\langle a \rangle$ is the thickness-weighted zonal-mean and $\underline{a}$ is the depth-mean of diagnostic $a$. Symbol | represents the deviation from the zonal-depth-mean, and symbol † represents the deviation from the zonal mean. The meridional heat transport components integrated over the whole ocean depth ($D$) can be written as

$$MHT_{over(z)}(y,t) = \rho_0 C_p \int_{-D}^{0} \int_{x_w}^{x_e} \langle v \rangle^{|}(z,y,t) \langle \theta \rangle^{|}(z,y,t) \mathrm{d}x \mathrm{d}z, \tag{7}$$

$$MHT_{gyre(z)}(y,t) = \rho_0 C_p \int_{-D}^{0} \int_{x_w}^{x_e} v^{\dagger}(z,x,y,t) \theta^{\dagger}(z,x,y,t) \mathrm{d}x \mathrm{d}z, \tag{8}$$

$$MHT_{over(\sigma)}(y,t) = \rho_0 C_p \int_{\sigma_{\min}}^{\sigma_{\max}} \int_{x_w}^{x_e} \langle v \rangle^{|}(\sigma,y,t) \langle \theta \rangle^{|}(\sigma,y,t) \mathrm{d}x \mathrm{d}\sigma, \tag{9}$$

$$MHT_{iso(\sigma)}(y,t) = \rho_0 C_p \int_{\sigma_{\min}}^{\sigma_{\max}} \int_{x_w}^{x_e} v^{\dagger}(\sigma,x,y,t) \theta^{\dagger}(\sigma,x,y,t) \mathrm{d}x \mathrm{d}\sigma. \tag{10}$$

Since expressions (7–9) only involve deviations from the zonal-depth mean values, the magnitudes of these heat transport terms are robust irrespective of dimensional units and the choice of the vertical coordinate (complete derivation is in Supporting Information S1).

Similar to the overturning circulation, the heat transport magnitude due to overturning, $MHT_{over}$, varies depending on the choice of the vertical coordinate. The climatological-mean $MHT_{over}$ is stronger in $\sigma-$space than in $z-$space (Figures 4d and 4j). In $z-$space, the overturning component dominates over the gyre component, $MHT_{gyre(z)}$, at latitudes south of 40°N, while the opposite occurs at higher latitudes. On the other hand, in $\sigma-$space, most of the heat transport is due to meridional overturning, $MHT_{over(\sigma)}$, and the heat transport due to zonal anomalies in meridional velocities and temperatures in isopycnal layers, $MHT_{iso(\sigma)}$, is relatively small. This different response in the subpolar ocean emerges because warm northward flows and relatively cold and dense southward flows exist at the same depths (Frajka-Williams et al., 2019). Consequently, $MHT_{over(\sigma)}$ largely captures contributions from both $MHT_{over(z)}$ and $MHT_{gyre(z)}$ (see Lozier et al., 2019).

It is valuable to analyze the vertical structures of the climatological meridional heat transport components, as the ocean heat transport response to the NAO may differ between the ocean surface and deep ocean. In $z-$space, $\mathrm{MHT}_{over(z)}$ changes sign near 35°N in the upper 100 m (Figures 4b and 4c), which is due to opposite directions of Ekman transport in the subtropical and subpolar regions (Williams et al., 2014). On the other hand, both subtropical and subpolar gyres transport heat northwards. In $\sigma-$space, the heat transport due to overturning near the surface (lightest waters) is largely northwards (Figure 4h), which is due to the combined effect of surface Ekman cells and ocean gyres. At densities greater than 27.6 kg $m^{-3}$, the geostrophic component of the overturning circulation carries heat northward. The relatively small heat transport due to the isopycnal component is mainly at latitudes north of 30° (Figure 4i).

The fast and slow responses due to the NAO forcing are also evident in the time-series of meridional heat transport anomalies (Figures 3d–3f and 3j–3l). There are notable differences in the behavior of the heat transport components depending on the vertical coordinate. In $z-$space, both overturning, $\mathrm{MHT}_{over(z)}$, and gyre, $\mathrm{MHT}_{gyre(z)}$, components contribute about equally to the heat transport change in the fast-response period. These rapid changes in heat transport are due to surface wind stress anomalies, which alter the overturning and gyre volume transports leading to changes in net heat transport. During the slow-response period, however, $\mathrm{MHT}_{gyre(z)}$ explains the majority change in heat transport. NAO forcing creates opposing-signed subtropical and subpolar SST anomalies (Figure 1), which are redistributed via the ocean circulation in the slow-response period. In principle, changes in $\mathrm{MHT}_{gyre(z)}$ can arise either via changes in gyre volume transport or changes in east-west temperature gradients. To examine their contributions, $\mathrm{MHT}_{gyre(z)}$ is further decomposed (Figures 3e and 3k, see Supporting Information S1 for derivations). The first component, $\mathrm{MHT}'_{gyre(z)} : \left[v^{\dagger} - \overline{v^{\dagger}}\right]\left[\overline{\theta^{\dagger}}\right]$, is the anomalous $\mathrm{MHT}_{gyre(z)}$ due to temporal changes in gyre volume transport only and is the main cause for the anomalous gyre heat transport in the fast-response period. The gyre volume transport is modified by wind stress anomalies at the onset of NAO forcing. The second component, $\mathrm{MHT}'_{gyre(z)} : \left[\overline{v^{\dagger}}\right]\left[\theta^{\dagger} - \overline{\theta^{\dagger}}\right]$, is the anomalous $\mathrm{MHT}_{gyre(z)}$ due to changes in east-west temperature gradients only and is the dominant contributor to the anomalous $\mathrm{MHT}_{gyre(z)}$ in the slow-response period. In contrast, gyre volume transport anomalies vanish within a year of NAO onset and hence cannot cause delayed changes in heat transport (see Supporting Information S1). Thus, the persistent anomaly in $\mathrm{MHT}_{gyre(z)}$ in the slow-response period is primarily due to the redistribution of subtropical temperature anomalies into the subpolar region and the resulting modifications in the east-west temperature gradients.

In $\sigma-$space decomposition, the overturning component, $MHT_{over(\sigma)}$, captures the majority of the variability in heat transport (Figure 3). The relatively small anomaly in the isopycnal component, $MHT_{iso(\sigma)}$, first appears a few months after the onset of NAO forcing (Figures 3f and 3l). Unlike anomalies in the overturning and gyre heat transport components, $\mathrm{MHT}_{iso(\sigma)}$ anomaly has the same sign during both the fast and slow response periods. Since $\mathrm{MHT}_{iso(\sigma)}$ is caused by zonal temperature gradients within isopycnal layers, the redistribution of temperature anomalies is required to cause variations in the isopycnal heat transport component. Thus, the anomalous isopycnal heat transport is a consequence of the slow ocean response only.

### 3.3. Fast and Slow Timescales

The fast ocean response to a winter NAO event only lasts for winter–spring seasons, whereas the delayed, slow ocean response persists for 2–3 years. As a result of the delayed response, there is a time lag between the onset of NAO forcing and anomalies in the geostrophic component of the overturning at 50°N of 1–3 years. The time lag between the onset of NAO forcing and subpolar SST anomalies, which peak when the cumulative sums of anomalies in heat flux and heat convergence show little variations, is about 3–4 years (Figure 3).

Several studies have looked into time-lag relationships between different atmospheric and oceanic indices. Desbruyères et al. (2019) found a time lag of about 5 years between surface water-mass transformation in the subpolar ocean and meridional overturning at 45°N in in situ hydrographic data sets. Yeager et al. (2021) observed a similar time lag between deep water formation in the Labrador sea and meridional overturning at 45°N in high-resolution climate model simulations. Fraser and Cunningham (2021) constructed a time-series for the meridional overturning strength for the last 120 years and showed that the overturning at 50°N leads the mean North Atlantic SST by 2–3 years.

These time lags in previous studies are consistent with our analyses, which suggest that the North Atlantic ocean's memory of atmospheric forcing is about 4–5 years. However, NAO forcing persisting in consecutive years can increase the time lag between the onset of the NAO and ocean-based indices (Kloewer et al., 2014; Lohmann et al., 2009a; Robson et al., 2012). For example, Eden and Willebrand (2001) forced an ocean model using constant NAO+ forcing and found that the delayed strengthening in the meridional overturning occurs 6–8 years after the onset of NAO+ forcing. This longer timescale is because it takes a few years for the strengthening in the geostrophic component of the overturning to compensate for the decline in the overturning strength due to constantly imposed anomalous Ekman transport. The ocean circulation continuously redistributes temperature anomalies created via heat flux anomalies associated with the NAO and modifies east-west temperature gradients. Consequently, it could take almost a decade for positive SST anomalies to appear in the subpolar ocean due to persistent NAO+ forcing. The advantage of our ensemble-based approach is that the time-lag magnitudes from a single NAO event can be precisely computed without being required to run artificial perturbation experiments as applied in previous studies (Eden & Willebrand, 2001; Lohmann et al., 2009b).

## 4. Conclusions

The North Atlantic Oscillation (NAO) plays a key role in determining the ocean variability in the North Atlantic (Marshall, Kushnir, et al., 2001). In the present study, climate model ensemble hindcasts were employed to investigate the impacts of a single NAO event on the subpolar ocean on seasonal to inter-annual timescales.

The ocean response to winter NAO forcing in the subpolar North Atlantic can be understood as a combination of a fast response and a delayed slow response. The fast ocean response depicts the immediate NAO impact on the oceans and lasts for winter–spring seasons, during which both surface wind stress and air-sea heat flux anomalies associated with the NAO forcing contribute nearly equally to changes in the ocean state. For example, NAO+ forcing leads to anomalous cooling and weakening in the overturning circulation and northward heat transport via changes in Ekman transport and ocean-atmosphere heat exchanges in the subpolar region (Eden & Willebrand, 2001; Marshall, Kushnir, et al., 2001). During the slow-response period after the onset of a NAO+ event, the trend reverses, and instead, there is continuous warming of the upper ocean and strengthening of the overturning circulation. This warming trend persists for 2–3 years and is primarily achieved by enhanced heat convergence into the subpolar region. In the case of NAO− forcing, there are again opposing-signed trends, but this time involving rapid warming followed by slow continuous cooling in the subpolar ocean.

The anomalous heat convergence during the fast and slow responses is driven by anomalous northward heat transport connected to both meridional overturning and horizontal gyre circulations in depth-space analysis (also see Eden & Willebrand, 2001; Williams et al., 2015). In density space, on the other hand, the anomalous northward heat transport is primarily linked to meridional overturning, which combines the overturning and gyre transports computed in depth-space, and the contribution from the isopycnal heat transport component is relatively small. Overall, the choice of the vertical coordinate affects the interpretation of how the subpolar ocean variability is controlled.

From the perspective of ocean dynamics, the fast ocean response is primarily wind-driven and ageostrophic in nature, whereas the slow response is related to the geostrophic flow component in the subpolar region. Eden and Willebrand (2001) argue that the delayed ocean response due to NAO forcing can be understood in terms of buoyancy-driven changes in the subpolar gyre circulation, which then affect east-west pressure gradients modifying the strength of the meridional overturning circulation (also see Lozier et al., 2010; Williams et al., 2015). In our analysis, however, the delayed ocean response is related to the formation of opposing-signed surface temperature anomalies in the subtropical and subpolar oceans due to NAO forcing, rather than changes in the subpolar gyre volume transport. The redistribution of these temperature anomalies then modifies the boundary density contrasts, overturning circulation and northward heat transport (e.g., see Roussenov et al., 2022).

As a result of the slow ocean response, the positive or negative anomalies in surface temperatures in the subpolar region peak in amplitude at a time lag of 4–5 years from the onset of NAO+ or NAO− forcing, respectively. On the other hand, the time lag between the onset of an NAO event and the geostrophic overturning response extends from 2 to 3 years. These time-lags are generally consistent with previous studies that examined the time-lag relationships among different indices based on the ocean and atmospheric states (Desbruyères et al., 2019; Fraser & Cunningham, 2021; Yeager et al., 2021). In contrast, idealized experiments forced with persistent NAO forcing report a slow ocean-adjustment timescale of 6–8 years (Eden & Willebrand, 2001; Lohmann et al., 2009b). These perturbation experiments involve a shift in the mean climate state as the oceans slowly adjust to the NAO forcing that is kept constant in time, and the slow adjustment is achieved through a combination of slow and fast ocean responses occurring throughout the simulations. Hence, this combined ocean-adjustment timescale to persistent forcing is fundamentally different from the slow-response timescale of 3–4 years to a single NAO event in our ensemble-based approach.

The subpolar ocean develops reversing-signed sea surface temperature anomalies in time due to the opposing effects of the fast and slow ocean responses to a single NAO event. These temperature anomalies can persist for several years, which may feedback on the atmosphere by modifying the air-sea heat exchange (Peings et al., 2016; Sutton & Dong, 2012). This inter-annual ocean variability and resulting feedback may then be important for predicting regional climate.

## Conflict of Interest

The authors declare no conflicts of interest relevant to this study.

## Data Availability Statement

Post-processed data and python scripts used in the analysis are available at Khatri (2022).

**Acknowledgments**
We thank two anonymous reviewers for their valuable comments. The work is part of "Subpolar North Atlantic Processes—Dynamics and Predictability of Variability in Gyre and Overturning" project and is funded by Natural Environment Research Council (NERC) Grant NE/T013494/1. JASMIN (http://jasmin.ac.uk/) and CEDA (www.ceda.ac.uk/) facilities were used for the computations. **xarray** (Hoyer & Hamman, 2017), **xgcm** (Abernathey et al., 2022) and **dask** (Matthew Rocklin, 2015) python packages were very helpful in our analyses. DMS was supported by the Met Office Hadley Centre Climate Programme funded by BEIS and Defra.

## References

Abernathey, R. P., Busecke, J. J. M., Smith, T. A., Deauna, J. D., Banihirwe, A., Nicholas, T., et al. (2022). xgcm: General circulation model postprocessing with xarray. *Zenodo*. https://doi.org/10.5281/zenodo.6643579

Barrier, N., Cassou, C., Deshayes, J., & Treguier, A.-M. (2014). Response of North Atlantic Ocean circulation to atmospheric weather regimes. *Journal of Physical Oceanography*, *44*(1), 179–201. https://doi.org/10.1175/JPO-D-12-0217.1

Boer, G. J., Smith, D. M., Cassou, C., Doblas-Reyes, F., Danabasoglu, G., Kirtman, B., et al. (2016). The decadal climate prediction project (DCPP) contribution to CMIP6. *Geoscientific Model Development*, *9*(10), 3751–3777. https://doi.org/10.5194/gmd-9-3751-2016

Dee, D. P., Uppala, S. M., Simmons, A. J., Berrisford, P., Poli, P., Kobayashi, S., et al. (2011). The ERA-interim reanalysis: Configuration and performance of the data assimilation system. *Quarterly Journal of the Royal Meteorological Society*, *137*(656), 553–597. https://doi.org/10.1002/qj.828

Desbruyères, D. G., Mercier, H., Maze, G., & Daniault, N. (2019). Surface predictor of overturning circulation and heat content change in the subpolar North Atlantic. *Ocean Science*, *15*(3), 809–817. https://doi.org/10.5194/os-15-809-2019

Eden, C., & Jung, T. (2001). North Atlantic interdecadal variability: Oceanic response to the North Atlantic Oscillation (1865–1997). *Journal of Climate*, *14*(5), 676–691. https://doi.org/10.1175/1520-0442(2001)014⟨0676:NAIVOR⟩2.0.CO;2

Eden, C., & Willebrand, J. (2001). Mechanism of interannual to decadal variability of the North Atlantic circulation. *Journal of Climate*, *14*(10), 2266–2280. https://doi.org/10.1175/1520-0442(2001)014⟨2266:MOITDV⟩2.0.CO;2

Frajka-Williams, E., Ansorge, I. J., Baehr, J., Bryden, H. L., Chidichimo, M. P., Cunningham, S. A., et al. (2019). Atlantic meridional overturning circulation: Observed transport and variability. *Frontiers in Marine Science*, *260*. https://doi.org/10.3389/fmars.2019.00260

Fraser, N. J., & Cunningham, S. A. (2021). 120 years of AMOC variability reconstructed from observations using the Bernoulli inverse. *Geophysical Research Letters*, *48*(18), e2021GL093893. https://doi.org/10.1029/2021GL093893

Hall, M. M., & Bryden, H. L. (1982). Direct estimates and mechanisms of ocean heat transport. Deep Sea Research Part A. *Oceanographic Research Papers*, *29*(3), 339–359. https://doi.org/10.1016/0198-0149(82)90099-1

Hansen, D. V., & Bezdek, H. F. (1996). On the nature of decadal anomalies in North Atlantic sea surface temperature. *Journal of Geophysical Research*, *101*(C4), 8749–8758. https://doi.org/10.1029/95JC03841

Hieronymus, M., & Nycander, J. (2013). The budgets of heat and salinity in NEMO. *Ocean Modelling*, *67*, 28–38. https://doi.org/10.1016/j.ocemod.2013.03.006

Hoyer, S., & Hamman, J. (2017). xarray: N-D labeled arrays and datasets in Python. *Journal of Open Research Software*, *5*(1), 10. https://doi.org/10.5334/jors.148

Hurrell, J. W. (1995). Decadal trends in the North Atlantic Oscillation: Regional temperatures and precipitation. *Science*, *269*(5224), 676–679. https://doi.org/10.1126/science.269.5224.676

Hurrell, J. W., & Deser, C. (2010). North Atlantic climate variability: The role of the North Atlantic Oscillation. *Journal of Marine Systems*, *79*(3–4), 231–244. https://doi.org/10.1016/j.jmarsys.2009.11.002

Jackson, L. C., Biastoch, A., Buckley, M. W., Desbruyères, D. G., Frajka-Williams, E., Moat, B., & Robson, J. (2022). The evolution of the North Atlantic meridional overturning circulation since 1980. *Nature Reviews Earth & Environment*, *3*(4), 241–254. https://doi.org/10.1038/s43017-022-00263-2

Johnson, H. L., Cessi, P., Marshall, D. P., Schloesser, F., & Spall, M. A. (2019). Recent contributions of theory to our understanding of the Atlantic meridional overturning circulation. *Journal of Geophysical Research: Oceans*, *124*(8), 5376–5399. https://doi.org/10.1029/2019JC015330

Josey, S. A., & Sinha, B. (2022). Subpolar atlantic ocean mixed layer heat content variability is increasingly driven by an active ocean. *Communications Earth & Environment*, *3*(1), 1–8. https://doi.org/10.1038/s43247-022-00433-6

Khatri, H. (2022). Subpolar ocean variability analysis using DePreSys4 hindcast output. *Zenodo*. https://doi.org/10.5281/zenodo.7096231

Kloewer, M., Latif, M., Ding, H., Greatbatch, R. J., & Park, W. (2014). Atlantic meridional overturning circulation and the prediction of North Atlantic sea surface temperature. *Earth and Planetary Science Letters*, *406*, 1–6. https://doi.org/10.1016/j.epsl.2014.09.001

Lohmann, K., Drange, H., & Bentsen, M. (2009a). A possible mechanism for the strong weakening of the North Atlantic subpolar gyre in the mid-1990s. *Geophysical Research Letters*, *36*(15). https://doi.org/10.1029/2009GL039166

Lohmann, K., Drange, H., & Bentsen, M. (2009b). Response of the North Atlantic subpolar gyre to persistent North Atlantic Oscillation like forcing. *Climate Dynamics*, *32*(2), 273–285. https://doi.org/10.1007/s00382-008-0467-6

Lozier, M. S., Leadbetter, S., Williams, R. G., Roussenov, V., Reed, M. S., & Moore, N. J. (2008). The spatial pattern and mechanisms of heat-content change in the North Atlantic. *Science*, *319*(5864), 800–803. https://doi.org/10.1126/science.1146436

Lozier, M. S., Li, F., Bacon, S., Bahr, F., Bower, A. S., Cunningham, S., et al. (2019). A sea change in our view of overturning in the subpolar North Atlantic. *Science*, *363*(6426), 516–521. https://doi.org/10.1126/science.aau6592

Lozier, M. S., Roussenov, V., Reed, M. S., & Williams, R. G. (2010). Opposing decadal changes for the North Atlantic meridional overturning circulation. *Nature Geoscience*, *3*(10), 728–734. https://doi.org/10.1038/ngeo947

Marshall, J., Johnson, H., & Goodman, J. (2001). A study of the interaction of the North Atlantic Oscillation with ocean circulation. *Journal of Climate*, *14*(7), 1399–1421. https://doi.org/10.1175/1520-0442(2001)014⟨1399:ASOTIO⟩2.0.CO;2

Marshall, J., Kushnir, Y., Battisti, D., Chang, P., Czaja, A., Dickson, R., et al. (2001). North Atlantic climate variability: Phenomena, impacts and mechanisms. *International Journal of Climatology: A Journal of the Royal Meteorological Society*, *21*(15), 1863–1898. https://doi.org/10.1002/joc.693

Menary, M. B., Jackson, L. C., & Lozier, M. S. (2020). Reconciling the relationship between the AMOC and Labrador Sea in OSNAP observations and climate models. *Geophysical Research Letters*, *47*(18), e2020GL089793. https://doi.org/10.1029/2020GL089793

O'Reilly, C. H., Zanna, L., & Woollings, T. (2019). Assessing external and internal sources of Atlantic multidecadal variability using models, proxy data, and early instrumental indices. *Journal of Climate*, *32*(22), 7727–7745. https://doi.org/10.1175/JCLI-D-19-0177.1

Peings, Y., Simpkins, G., & Magnusdottir, G. (2016). Multidecadal fluctuations of the North Atlantic Ocean and feedback on the winter climate in CMIP5 control simulations. *Journal of Geophysical Research: Atmospheres*, *121*(6), 2571–2592. https://doi.org/10.1002/2015JD024107

Robson, J., Ortega, P., & Sutton, R. (2016). A reversal of climatic trends in the North Atlantic since 2005. *Nature Geoscience*, *9*(7), 513–517. https://doi.org/10.1038/ngeo2727

Robson, J., Sutton, R., Lohmann, K., Smith, D., & Palmer, M. D. (2012). Causes of the rapid warming of the North Atlantic Ocean in the mid-1990s. *Journal of Climate*, *25*(12), 4116–4134. https://doi.org/10.1175/JCLI-D-11-00443.1

Rocklin, M. (2015). Dask: Parallel computation with blocked algorithms and task scheduling. In K. Huff & B. James (Eds.), *Proceedings of the 14th Python in science conference* (pp. 126–132). https://doi.org/10.25080/Majora-7b98e3ed-013

Roussenov, V. M., Williams, R. G., Lozier, M. S., Holliday, N. P., & Smith, D. M. (2022). Historical reconstruction of subpolar North Atlantic overturning and its relationship to density. *Journal of Geophysical Research: Oceans*, *127*(6), e2021JC017732. https://doi.org/10.1029/2021JC017732

Siedler, G., Gould, J., & Church, J. (2001). *Ocean circulation and climate: Observing and modelling the global ocean*. Elsevier.

Smith, D. M., Allan, R. P., Coward, A. C., Eade, R., Hyder, P., Liu, C., et al. (2015). Earth's energy imbalance since 1960 in observations and CMIP5 models. *Geophysical Research Letters*, *42*(4), 1205–1213. https://doi.org/10.1002/2014GL062669

Smith, D. M., & Murphy, J. M. (2007). An objective ocean temperature and salinity analysis using covariances from a global climate model. *Journal of Geophysical Research*, *112*(C2), C02022. https://doi.org/10.1029/2005JC003172

Sutton, R. T., & Dong, B. (2012). Atlantic Ocean influence on a shift in European climate in the 1990s. *Nature Geoscience*, *5*(11), 788–792. https://doi.org/10.1038/ngeo1595

Thomson, R. E., & Emery, W. J. (2014). *Data analysis methods in physical oceanography*. Newnes.

Visbeck, M., Cullen, H., Krahmann, G., & Naik, N. (1998). An ocean model's response to North Atlantic Oscillation-like wind forcing. *Geophysical Research Letters*, *25*(24), 4521–4524. https://doi.org/10.1029/1998GL900162

Williams, R. G., Roussenov, V., Lozier, M. S., & Smith, D. (2015). Mechanisms of heat content and thermocline change in the subtropical and subpolar North Atlantic. *Journal of Climate*, *28*(24), 9803–9815. https://doi.org/10.1175/JCLI-D-15-0097.1

Williams, R. G., Roussenov, V., Smith, D., & Lozier, M. S. (2014). Decadal evolution of ocean thermal anomalies in the North Atlantic: The effects of Ekman, overturning, and horizontal transport. *Journal of Climate*, *27*(2), 698–719. https://doi.org/10.1175/JCLI-D-12-00234.1

Woollings, T., Hannachi, A., & Hoskins, B. (2010). Variability of the North Atlantic eddy-driven jet stream. *Quarterly Journal of the Royal Meteorological Society*, *136*(649), 856–868. https://doi.org/10.1002/qj.625

Yang, C., Masina, S., Bellucci, A., & Storto, A. (2016). The rapid warming of the North Atlantic Ocean in the mid-1990s in an eddy-permitting ocean reanalysis (1982–2013). *Journal of Climate*, *29*(15), 5417–5430. https://doi.org/10.1175/JCLI-D-15-0438.1

Yeager, S., Castruccio, F., Chang, P., Danabasoglu, G., Maroon, E., Small, J., et al. (2021). An outsized role for the Labrador Sea in the multidecadal variability of the Atlantic overturning circulation. *Science Advances*, *7*(41). eabh3592. https://doi.org/10.1126/sciadv.abh3592

Zhao, J., & Johns, W. (2017). Basinwide response of the Atlantic meridional overturning circulation to interannual wind forcing. *Climate Dynamics*, *49*(11), 4263–4280. https://doi.org/10.1002/2013JC009407

Zou, S., Lozier, M. S., & Xu, X. (2020). Latitudinal structure of the meridional overturning circulation variability on interannual to decadal time scales in the North Atlantic Ocean. *Journal of Climate*, *33*(9), 3845–3862. https://doi.org/10.1175/JCLI-D-19-0215.1